Int j simul model 21 (2022) 3, 513-524
Original scientific paper

STATIC CONTACT MODELLING AND ANALYSIS FOR RAIL GRINDING WITH ABRASIVE BELT

Liu, Y.[*,**]; Fan, W. G.[*,**,#]; Zhang, X. L.[***]; Wu, Z. W.[*,**] & Wu, C. X.[*,**]

[*] School of Mechanical, Electronic and Control Engineering, Beijing Jiaotong University, Beijing 100044, P. R. China

[**] Key Laboratory of Vehicle Advanced Manufacturing, Measuring and Control Technology, Ministry of Education, Beijing Jiaotong University, Beijing 100044, P. R. China

[***] Dynamic Machinery Institute of Inner Mongolia, Inner Mongolia 010000, P. R. China

E-Mail: 20121243@bjtu.edu.cn, wgfan@bjtu.edu.cn, 15598226431@163.com, 20116002@bjtu.edu.cn, 21121250@bjtu.edu.cn ([#] Corresponding author)

Abstract

Rail grinding with abrasive belt is increasingly applied in daily rail maintenance due to its high efficiency and high quality. The contact between rail and abrasive belt largely determines grinding efficiency and grinding quality, but the influences of grinding process and contact wheel's parameters on the contact behaviour are obscure. To explore the influences, a finite element model of the wheel-rail contact was established. The simulation results showed that the grinding angle significantly affected the shape of contact spot. The contact spot gradually became narrower as the grinding angle increased. Similarly, the reduction of the contact wheel radius significantly increased the contact stress. But when the ratio of the thickness of rubber layer to wheel radius increased above 60 %, it had little effect on the size of contact spot and maximum contact stress. This study provides the basis for the selection of grinding process and contact wheel's parameters. In the actual grinding process, grinding process and contact wheel should be selected according to grinding requirements.

(Received in April 2022, accepted in June 2022. This paper was with the authors 2 weeks for 1 revision.)

Key Words: Rail Grinding, Abrasive Belt, Contact, Stress Distribution

1. INTRODUCTION

Due to the development of rail transit systems, the speed and axle weight of trains increase, and rail surface defects are gradually more prominent [1, 2], such as corrugation, cracks, and scratches [3-5]. If these defects are not processed in time, the state of wheel-rail contact will deteriorate, thus seriously affecting the smooth operation of trains and passenger comfort and even causing major safety accidents and casualties. Currently, the rail grinding technology is widely used to maintain rails around the world [6, 7]. In view of the advantages of abrasive belt grinding technology, the rail grinding with abrasive belt has been proposed [8-10]. As a new repair technology of rail surface defects, it has been gradually applied due to the advantages of high efficiency, high quality, safety, and environmental protection.

In the rail grinding with abrasive belt, the complex nonlinear contact interactions exist among contact wheel, abrasive belt, and rail. The contact behaviour of rail grinding with abrasive belt is significant because it affects material removal, grinding temperature rise, and residual stress, and determines grinding efficiency and grinding quality. It is necessary to explore the contact mechanism of wheel-rail in rail grinding with abrasive belt. Based on the surface morphology of abrasive belt, Fan et al. [11] established a microscopic contact pressure model and revealed the contact behaviour between abrasive grain and rail. Furthermore, Fan et al. [12] established a contact pressure model, obtained the boundary curve and stress distribution of the contact zone between rubber wheel and rail, and conducted finite element simulation and grinding test. In order to explore the static contact behaviour between concave contact wheel and rail, Wang et al. [13] converted the three-dimensional contact problem into a two-dimensional problem, so as to obtain the boundary curve function and stress distribution of the contact zone. Moreover, Wang et al. [14] established a numerical contact model of the local geometric relationship between the contact wheel and the surface of the rail and verified the accuracy of the established model through finite element analysis. In the grinding process of aero-engine blades, Xiao et al. [15] established a finite element model of multi-particle belt grinding under different process parameters and carried out the critical belt grinding experiment to study the distribution characteristics of residual stress on the surface after grinding. In addition, Vigneashwara et al. [16] conducted experimental tests with the Taguchi method and found that the material removed from the surface during the grinding by abrasive belt had a nonlinear relationship with various process parameters. Existing studies on the contact behaviours between contact wheel, abrasive belt, and rail were mainly focused on the establishment of accurate contact models with various methods. The influences of grinding process and contact wheel's parameters need to be further studied.

Inspired by the prominent role of finite element model in the field of engineering [17-19], we analysed the influence of grinding process and contact wheel's parameters on contact behaviour. Firstly, rail grinding with abrasive belt is introduced, including the principle of rail grinding with abrasive belt and the contact behaviour. Then, a finite element model of rail grinding with abrasive belt was established. Finally, the influences of grinding process and contact wheel's parameters on the contact stress in rail grinding with abrasive belt was analysed by the above model.

2. CONTACT ANALYSIS IN RAIL GRINDING WITH ABRASIVE BELT

The basic principle of rail grinding with abrasive belt is shown in Fig. 1. The contact wheel consists of a hub and a rubber layer wrapped around the hub. The force is applied to the contact wheel in the grinding process and the particles of abrasive belt slides on the rail surface to achieve material cutting and removal [20, 21]. To complete the repair of rail surface, several grinding units are arranged in the direction of the rail extension to achieve enveloping grinding of the rail.

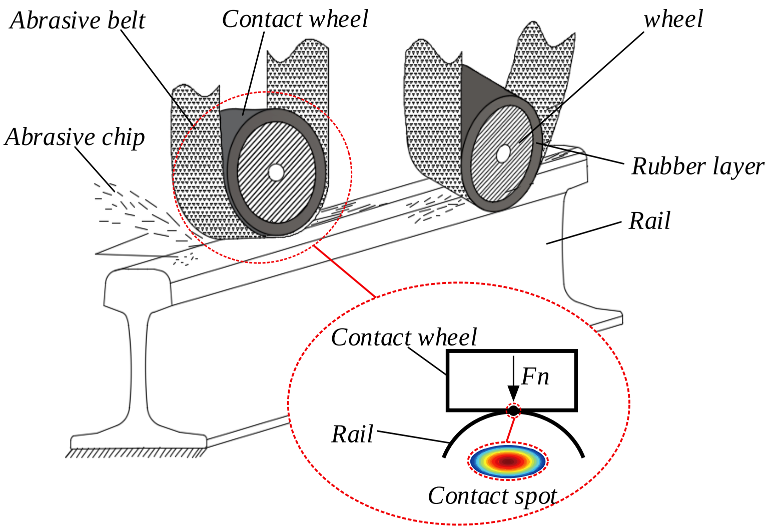

Figure 1: Schematic diagram of rail grinding with abrasive belt.

The paper aims to explore the effects of grinding process and contact wheel's parameters on contact stress. The main determinant of the formation and distribution of contact spots is contact wheel in rail grinding with abrasive belt, whereas the abrasive belt can be ignored. Therefore, this paper only considers contact wheel and rail, and the contact is transformed into the contact between contact wheel and rail.

3. DESCRIPTIONS AND SIMULATION PARAMETERS

3.1 Selection of rubber layer material

The rubber layer material of the contact wheel is a hyper-elastic material. The relationship between stress and strain of the hyper-elastic rubber does not follow Hooke's law. The relationship between stress and strain is a nonlinear relationship and the constitutive theory of rubber is usually determined by the strain energy function [22-24]. ABAQUS software has the significant nonlinear problem handling ability, so the Mooney-Rivlin material model in ABAQUS was selected.

3.2 Finite element model

In the finite element analysis, a standard rail of 60 kg/m was simulated. The rubber layer and the hub were bound and constrained. The mesh of the main contact zone was further refined. The specific finite element calculation model is shown in Fig. 2. The elastic modulus of the contact wheel hub and rail in the model was larger than that of the rubber layer. The rubber layer was adhered to the contact wheel hub, and the contact wheel and the rail were in the frictionless contact.

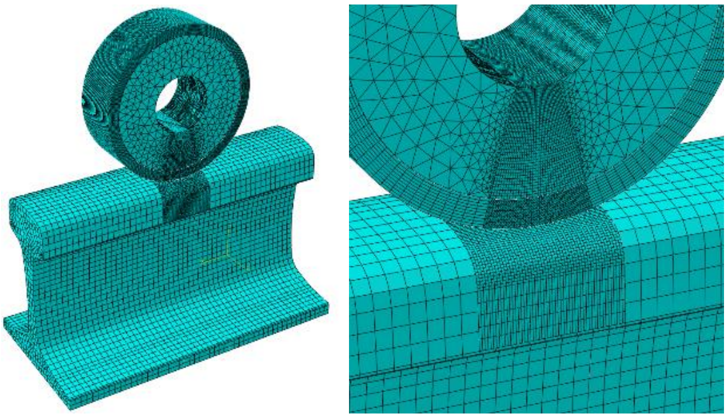

Figure 2: Finite element calculation model.

The material parameters used in the simulation are provided in Table I. The aluminium alloy of the contact wheel has the elastic modulus of 69 GPa and the Poisson's ratio of 0.34. The elastic modulus of the rail is 214 GPa and the Poisson's ratio of the rail is 0.3.

Table I: Rubber material simulation parameters.

Shore hardness -A [°]	**Elastic modulus** [N/mm^2]	**Modulus of shear** [N/mm^2]	**C_{10}** [N/mm^2]	**C_{01}** [N/mm^2]
40	1.381	0.452	0.181	0.045
50	2.397	0.755	0.302	0.076
60	4.268	1.185	0.474	0.118
70	7.289	1.839	0.736	0.184

4. RESULTS AND DISCUSSION

4.1 Effect of grinding pressure on contact stress

Under the conditions of contact wheel radius (R_w = 75 mm), rubber layer thickness (D = 10 mm), rubber layer hardness (HS = 60°), grinding angle (Deg = 0°), and different grinding pressures (F_n = 10 N, 25 N, 50 N, 75 N, 100 N, 125 N and 150 N), the finite element analysis was performed. The simulation results are shown in Fig. 3 and the variations of contact parameters with grinding pressure are shown in Fig. 4.

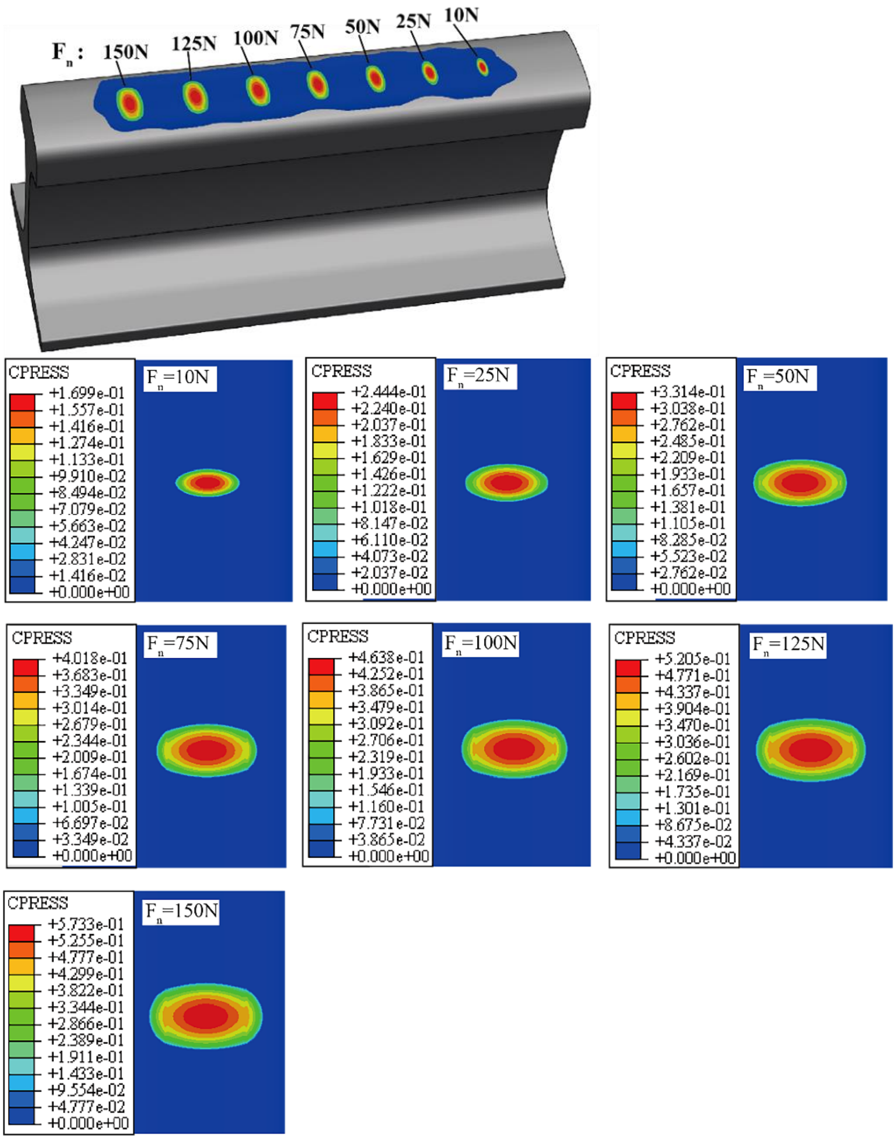

Figure 3: Contact spots under different grinding pressures.

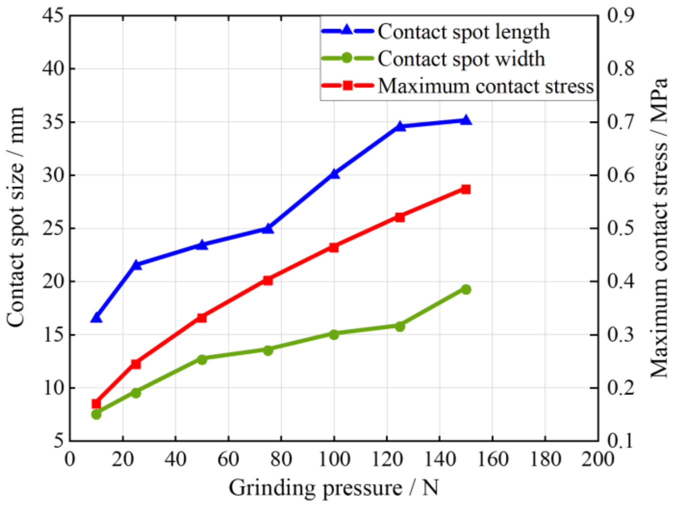

Figure 4: Variation of contact parameters with grinding pressure.

With the increase in grinding pressure, the contact zone and the maximum contact stress increased (Figs. 3 and 4). The shapes of the contact spots were substantially similar. However, when $F_n \geq 75$ N, the stress concentration phenomenon occurred on both sides of the contact spot. The phenomenon might be interpreted as follows. With the increase in the grinding pressure, the deformation of the contact wheel increased and the contact zone between contact wheel and rail surface became larger, thus increasing the curvature change in the contact zone.

4.2 Effect of grinding angle on contact stress

Under the conditions of contact wheel radius ($R_w = 75$ mm), rubber layer thickness ($D = 10$ mm), rubber layer hardness ($HS = 60°$), grinding pressure ($F_n = 50$ N), and different grinding angles ($Deg = 0.5°$, 1°, 2°, 10°, 12°, 14°, 20°, 40°, and 60°), the finite element analysis was performed. The simulation results are shown in Fig. 5 and the variations of contact parameters with grinding angle are shown in Fig. 6.

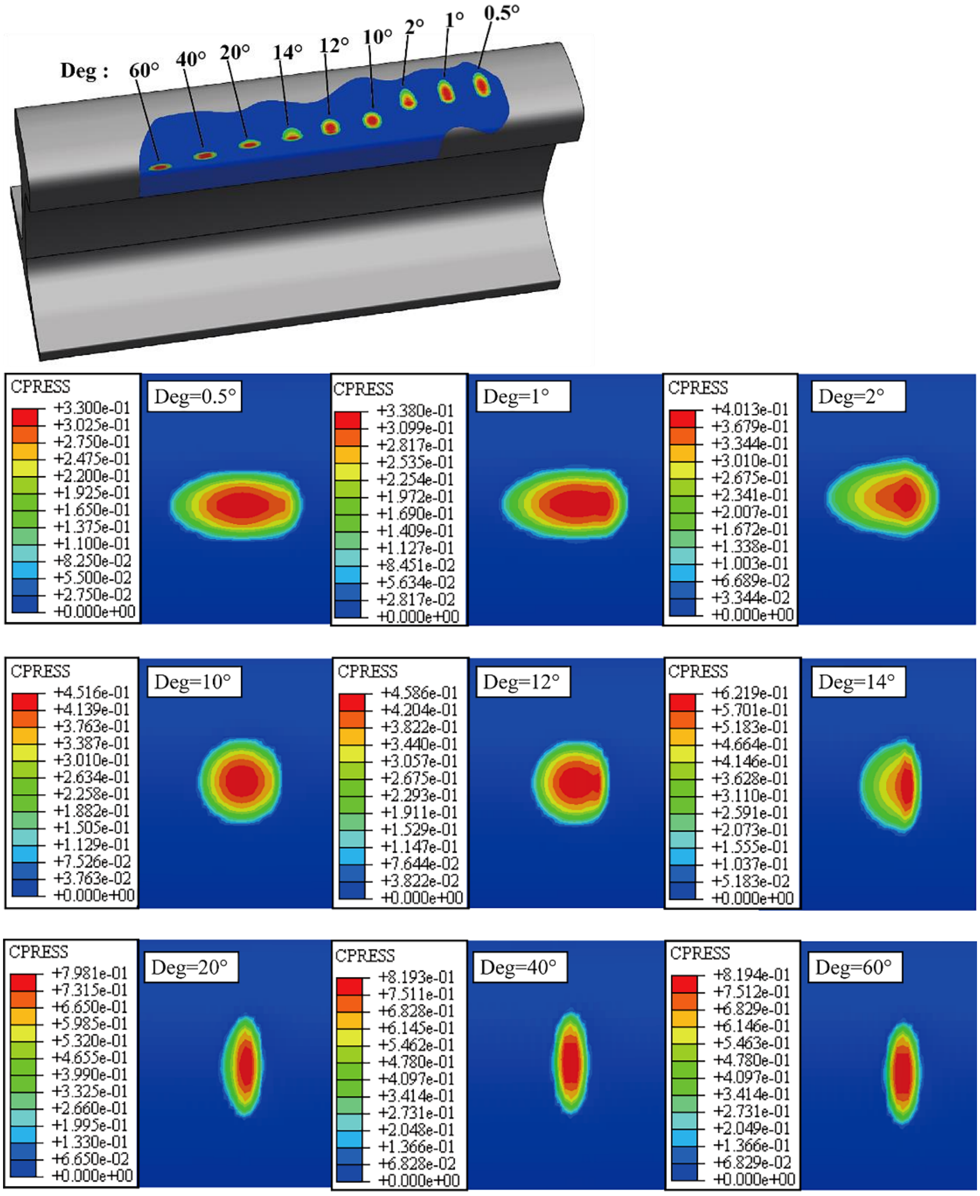

Figure 5: Contact spots under different grinding angles.

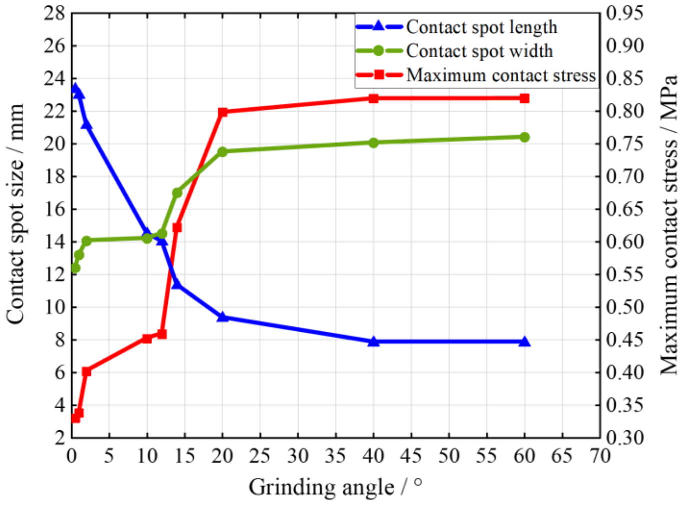

Figure 6: Variations of contact parameter with grinding angle.

The shape of the contact spot varied with grinding angle (Fig. 5). The variation is discussed as follows. The rail is composed of circular arcs with different curvatures. Therefore, the curvature in the contact zone varied with grinding angle. When the curvature in the contact zone was fixed (grinding angle = 0°, 40°, or 60°), the shapes of the contact spots were a regular ellipse. However, with the variation in curvature, the shapes of contact spots were no longer regular, as confirmed by the segmentation of the curve in Fig. 6. Under different grinding angles, it is important to choose an appropriate grinding strategy so as to avoid unnecessary damage to the rail.

4.3 Effect of the radius of contact wheel on contact stress

Under the conditions of rubber layer hardness ($HS = 60°$), grinding pressure ($F_n = 50$ N), rubber layer thickness ($D = 10$ mm), grinding angle ($Deg = 0°$), and different contact wheel radii (R_w = 25 mm, 50 mm, 75 mm, 100 mm, 125 mm, and 150 mm), the finite element analysis was performed. The simulation results are shown in Fig. 7 and the variations of contact parameters with contact wheel radius are shown in Fig. 8.

When $R_w = 125$ mm, a significant stress concentration phenomenon was observed on both sides of the contact spot (Fig. 7). The phenomenon might be interpreted as follows. Due to the structural change of the contact wheel, the contact zone became larger so that the curvature changed in the contact zone and resulted in stress concentration. Combined with Fig. 8, it can be found that as the radius of the contact wheel increased, the contact zone between contact wheel and rail surface became larger and the maximum contact stress between the contact wheel and rail surface was reduced.

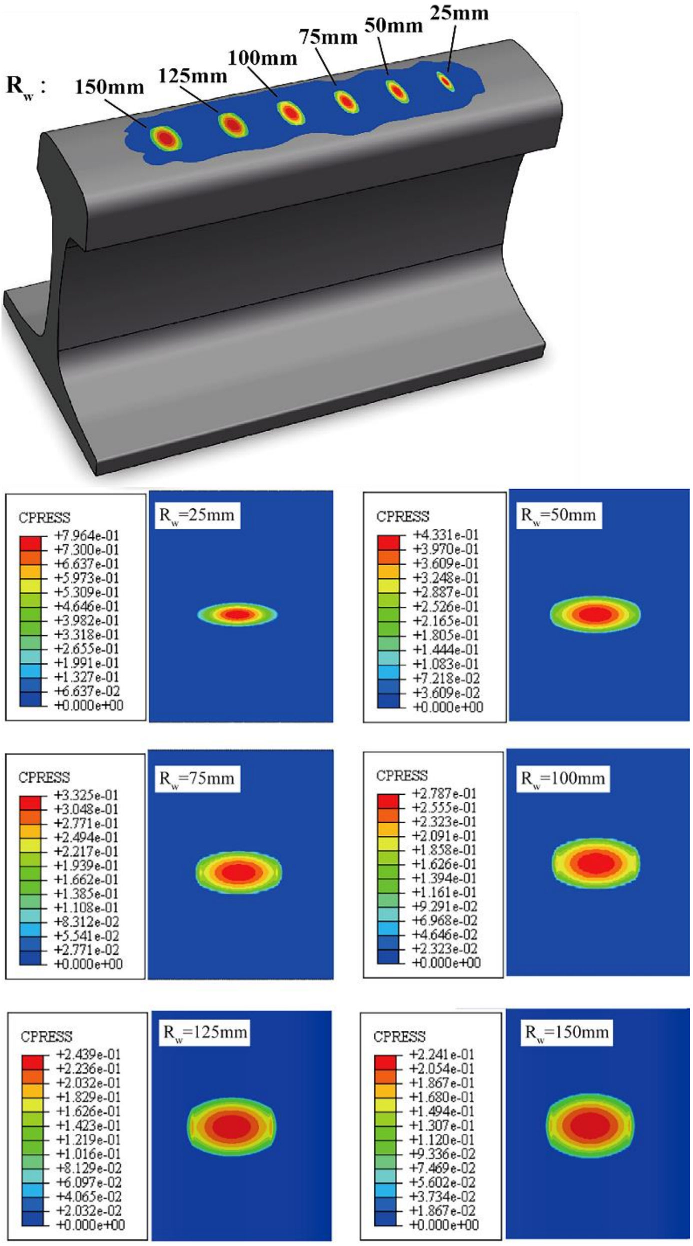

Figure 7: Contact spots under different contact wheel radii.

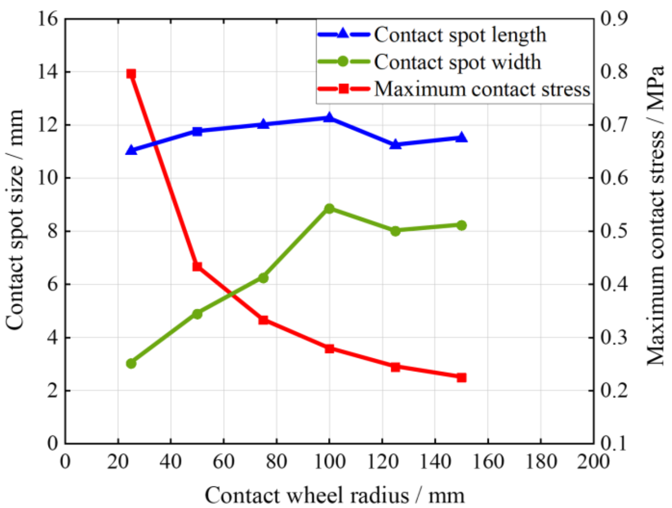

Figure 8: Variation of contact parameters with contact wheel radii.

4.4 Effect of the ratio of the thickness of rubber layer to wheel radius on contact stress

Under the conditions of contact wheel radius (R_w = 75 mm), rubber layer hardness (HS = 60°), grinding pressure (F_n = 50 N), grinding angle (Deg = 0°), and different ratios of the thickness of rubber layer to wheel radius (thickness ratio for short, 10 %, 20 %, 40 %, 60 %, 80 %, and 100 %), the finite element analysis was performed. The simulation results are shown in Fig. 9 and the variations of contact parameters with the thickness ratio are shown in Fig. 10.

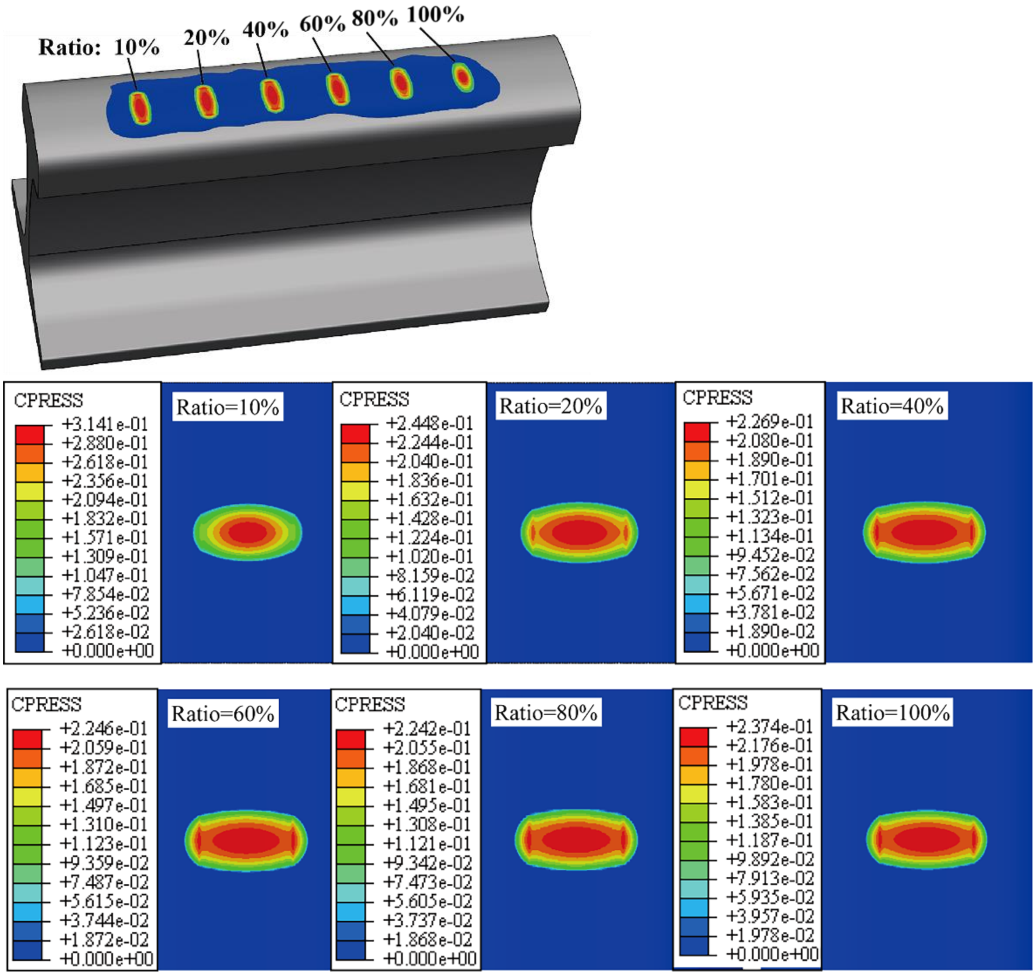

Figure 9: Contact spots under different thickness ratios of rubber layer.

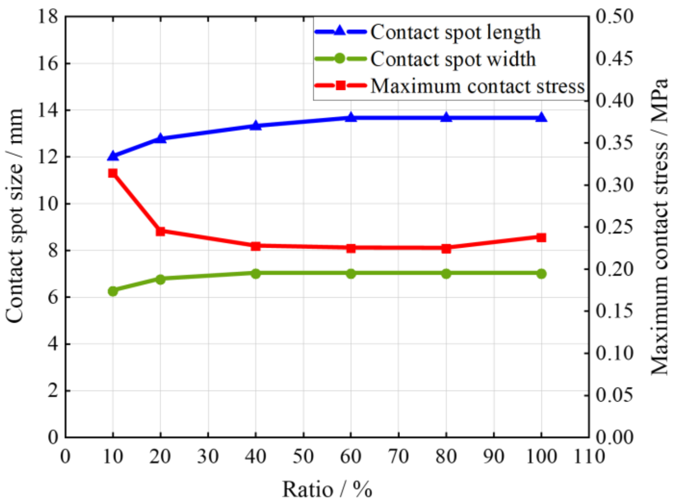

Figure 10: Variations of contact parameters with the thickness ratios of rubber layer.

When the thickness ratio increased from 20 % to 100 %, the significant stress concentration phenomenon was observed on both sides of the contact spot, indicating the curvature change in the contact zone (Fig. 9). The increase of thickness ratio affected the structural stiffness of the contact wheel, thus resulting in the greater deformation under the same grinding pressure. When the thickness ratio of the rubber layer increased, the size of contact zone gradually increased, but the maximum contact stress gradually decreased (Fig. 10). However, when the thickness ratio increased above 60 %, the contact zone was almost no longer changed.

4.5 Effect of the hardness of rubber layer on contact stress

Under the conditions of contact wheel radius (R_w = 75 mm), rubber layer thickness (D = 10 mm), grinding pressure (F_n = 50 N), grinding angle (Deg = 0°), and different Shore hardness (HS = 40°, 50°, 60°, and 70°), the finite element analysis was performed. The coefficients of the Mooney-Rivlin material model are shown in Table I. The simulation results are shown in Fig. 11 and the variations of contact parameters with the hardness of rubber layer are shown in Fig. 12.

With the increase in the hardness of rubber layer, the stress concentration phenomenon on both sides of the contact spot became less significant (Fig. 11). Due to the increase in the hardness of rubber layer, the contact zone between contact wheel and rail surface decreased and the curvature change in the contact zone was reduced. Moreover, as the hardness of rubber layer of contact wheel increased, the maximum contact stress increased (Fig. 12).

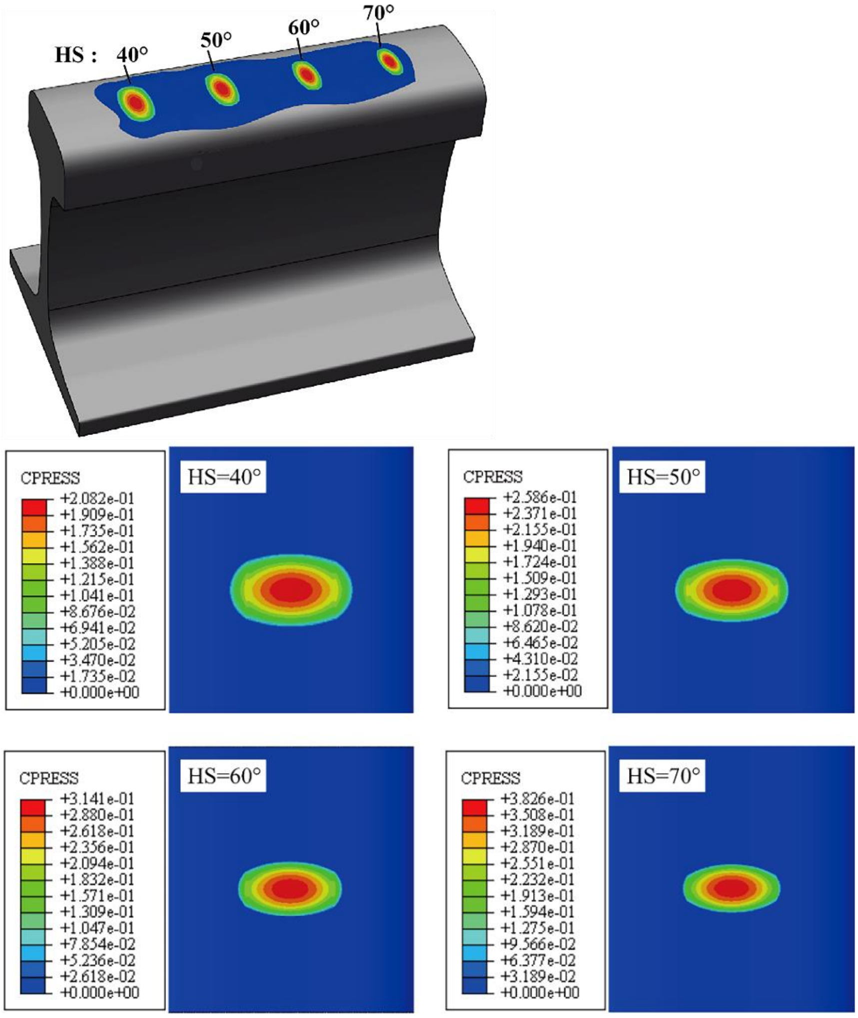

Figure 11: Contact spots under different hardness of rubber layer.

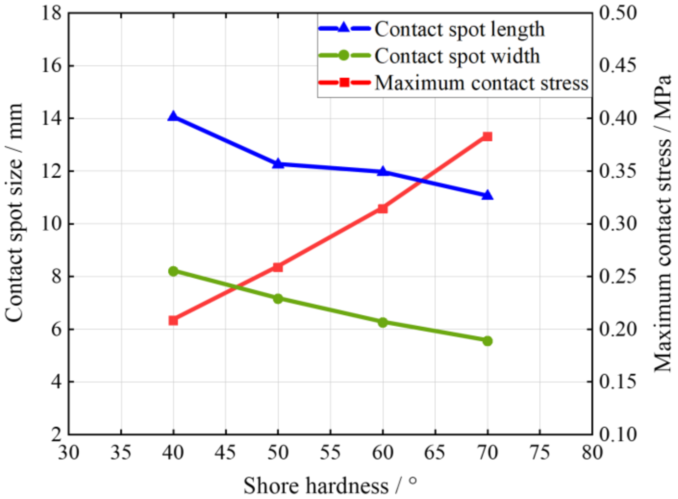

Figure 12: Variations of contact parameters with the hardness of rubber layer.

5. CONCLUSION

In order to study the influences of grinding process and contact wheel's parameters on the contact behaviour of contact wheel and rail, we established a static contact model for rail grinding with abrasive belt and performed the contact analysis with the finite element method. The simulation results showed that the shape of the contact spot was closely related to grinding angle. The contact spots under the same grinding angle had the similar shape. In addition, the maximum contact stress was sensitive to these parameters and reached 0.8194 MPa under the grinding angle of 60°, which is the maximum data measured. The reduction in the radius of the contact wheel also significantly increased the contact stress. Furthermore, the increase in thickness ratio tended to increase the occurrence of stress concentration on both sides of the contact spot. However, when the ratios of the thickness of rubber layer to wheel radius exceeded 60 %, its effects on the contact behaviour were small.

Due to some factors such as simulation can't fully simulate the actual environment, there may be some difference between the simulation prediction and the actual results. But this study partly provides some reference for the selection of contact wheels and grinding strategies. In the actual selection, the grinding strategy should be selected according to the actual grinding situation of rail damage. In addition, the radius of the contact wheel should be selected based on the size and damage of the grinding zone of rail so as to avoid the low grinding efficiency caused by the smaller material removal related to small radius or the waste of materials related to large radius. Moreover, the rubber layer with large hardness could be selected to enhance the grinding ability under ensuring buffer shock absorption.

In the further research, the surface characteristics of the abrasive belt, such as the type of abrasive grain, the size of abrasive grain and the density of abrasive grain, can also be considered, and experimental investigation can be carried out. This paper only studies the static contact of rail grinding with abrasive belt, and the dynamic contact behaviour can be further studied.

ACKNOWLEDGEMENT

The study was financially supported by the Fundamental Research Funds for the Central Universities (Grant No. 2019JBM050).

REFERENCES

[1] Sun, Y.; Guo, Y.; Lv, K.; Chen, M.; Zhai, W. (2019). Effect of hollow-worn wheels on the evolution of rail wear, *Wear*, Vol. 436-437, Paper 203032, 10 pages, doi:10.1016/j.wear.2019.203032

[2] Ding, H. H.; Fu, Z. K.; Wang, W. J.; Guo, J.; Liu, Q. Y.; Zhu, M. H. (2015). Investigation on the effect of rotational speed on rolling wear and damage behaviors of wheel/rail materials, *Wear*, Vol. 330-331, 563-570, doi:10.1016/j.wear.2014.12.043

[3] Du, X.; Jin, X.; Zhao, G.; Wen, Z.; Li, W. (2021). Rail corrugation of high-speed railway induced by rail grinding, *Shock and Vibration*, Vol. 2021, Paper 5546809, 14 pages, doi:10.1155/2021/5546809

[4] Jiang, W. J.; Liu, C.; He, C. G.; Guo, J.; Wang, W. J.; Liu, Q. Y. (2017). Investigation on impact wear and damage mechanism of railway rail weld joint and rail materials, *Wear*, Vol. 376-377, Part B, 1938-1946, doi:10.1016/j.wear.2017.02.035

[5] Ma, L.; Guo, J.; Liu, Q. Y.; Wang, W. J. (2017). Fatigue crack growth and damage characteristics of high-speed rail at low ambient temperature, *Engineering Failure Analysis*, Vol. 82, 802-815, doi:10.1016/j.engfailanal.2017.07.026

[6] Singleton, R.; Marshall, M. B.; Lewis, R.; Evans, G. (2015). Rail grinding for the 21st century – taking a lead from the aerospace industry, *Proceedings of the Institution of Mechanical Engineers, Part F: Journal of Rail and Rapid Transit*, Vol. 229, No. 5, 457-465, doi:10.1177/0954409714527929

[7] Tuzik, B. (2019). Refining approaches to corrective & preventative rail grinding, *Railway Track and Structures*, Vol. 115, No. 2, 14-23

[8] Fan, W. G.; Hou, G. Y.; Wang, W. X.; Wu, Y. F. (2019). Dynamic analysis of a novel rail-grinding car using open-structured abrasive belt for high-speed railways, *Mathematical Problems in Engineering*, Vol. 2019, Paper 1748679, 9 pages, doi:10.1155/2019/1748679

[9] Fan, W. G.; Hou, G. Y.; Wang, W. X.; Zhang, X. L.; Wang, J. D. (2019). Design and dynamic analysis of a new rail grinding device using closed abrasive belt, *International Journal of Simulation Modelling*, Vol. 18, No. 3, 531-542, doi:10.2507/IJSIMM18(3)CO14

[10] Fan, W. G.; Zhang, S.; Wang, J. D.; Wang, X. H.; Wang, W. X. (2019). Temperature field of open-structured abrasive belt rail grinding using FEM, *International Journal of Simulation Modelling*, Vol. 19, No. 2, 346-356, doi:10.2507/IJSIMM19-2-CO10

[11] Fan, W. G.; Wang, W. X.; Wang, J. D.; Zhang, X. L.; Qian, C.; Ma, T. F. (2020). Microscopic contact pressure and material removal modeling in rail grinding using abrasive belt, *Proceedings of the Institution of Mechanical Engineers, Part B: Journal of Engineering Manufacture*, Vol. 235, No. 1-2, 3-12, doi:10.1177/0954405420932419

[12] Fan, W. G.; Liu, Y. M.; Song, X. Y.; Cheng, J. F.; Li, J. Y. (2018). Influencing mechanism of rubber wheel on contact pressure and metal removal in corrugated rail grinding by abrasive belt, *Journal of Manufacturing Science and Engineering*, Vol. 140, No. 12, Paper 124501, 8 pages, doi:10.1115/1.4041243

[13] Wang, W. X.; Li, J. Y.; Fan, W. G. (2019). Investigation into static contact behavior in belt rail grinding using a concave contact wheel, *The International Journal of Advanced Manufacturing Technology*, Vol. 101, No. 9, 2825-2835, doi:10.1007/s00170-018-3049-8

[14] Wang, W. X.; Li, J. Y.; Fan, W. G.; Hou, G. Y. (2019). A numerical model to investigate contact status for rail grinding by abrasive belt with an axial deflection, *Journal of Brazilian Society of Mechanical Science and Engineering*, Vol. 41, No. 11, Paper 494, 10 pages, doi:10.1007/s40430-019-2006-2

[15] Xiao, G. J.; Song, K. K.; Zhou, H. W.; He, Y.; Dai, W. T. (2021). A multi-particle abrasive model for investigation of residual stress in belt grinding of titanium alloys, *Proceedings of the Institution of Mechanical Engineers, Part B: Journal of Engineering*, Vol. 235, No. 11, 1739-1750, doi:10.1177/09544054211007985

[16] Vigneashwara, P.; Wahyu, C.; Tagoeh, T.; Gunasekaran, P. (2017). Predictive modelling and analysis of process parameters on material removal characteristics in abrasive belt grinding process, *Applied Sciences*, Vol. 7, No. 4, Paper 363, 17 pages, doi:10.3390/app7040363

[17] Calvo Hernandez, A.; Sanz Bobi, J. de D.; Gomez Fernandez, J.; Badolato Martin, A. (2021). Vibration reduction on overhead contact rails: a simulation-optimization approach, *International Journal of Simulation Modelling*, Vol. 20, No. 2, 315-326, doi:10.2507/IJSIMM20-2-561

[18] Szurgott, P.; Bernacki, P. (2020). Modelling of steel-concrete bridges subjected to a moving high-speed train, *International Journal of Simulation Modelling*, Vol. 20, No. 1, 29-40, doi:10.2507/IJSIMM19-1-499

[19] Zhang, W. X.; Wong, K.; Morales, M.; Molpeceres, C.; Arnold, C. B. (2020). Implications of using two low-power continuous-wave lasers for polishing, *International Journal of Extreme Manufacturing*, Vol. 2, No. 3, Paper 035101, 9 pages, doi:10.1088/2631-7990/ab94c6

[20] Zhe, H.; Jianyong, L.; Yueming, L.; Meng, N.; Wengang, F. (2017). Investigating the effects of contact pressure on rail material abrasive belt grinding performance, *The International Journal of Advanced Manufacturing Technology*, Vol. 97, No. 1, 779-786, doi:10.1007/s00170-017-0498-4

[21] Zhao, C. Y.; Li, J. Y.; Fan, W. G.; Liu, Y. M.; Wang, W. X. (2020). Experimental and simulation research on residual stress for abrasive belt rail grinding, *The International Journal of Advanced Manufacturing Technology*, Vol. 109, No. 1, 129-142, doi:10.1007/s00170-020-05664-5

[22] Bazkiaei, A. K.; Shirazi, K. H.; Shishesaz, M. (2020). A framework for model base hyper-elastic material simulation, *Journal of Rubber Research*, Vol. 23, No. 4, 287-299, doi:10.1007/s42464-020-00057-5

[23] Korba, A. G.; Kumar, A.; Barkey, M. (2020). A hyper-elastic thermal aging constitutive model for rubber-like materials, *Journal of Elastomers & Plastics*, Vol. 52, No. 8, 677-700, doi:10.1177/0095244319883405

[24] Hajhashemkhani, M.; Hematiyan, M. R.; Goenezen, S. (2018). Identification of material parameters of a hyper-elastic body with unknown boundary conditions, *Journal of Applied Mechanics*, Vol. 85, No. 5, Paper 051006, 13 pages, doi:10.1115/1.4039170